


RESEARCH ARTICLE

Open Access



Spectroscopic and antibacterial activities of cobalt and nickel nanoparticles: a comparative analysis

Sheriff A. Balogun^{1,2}, Tesleem O. Abolarinwa³, Funmilola A. Adesanya^{1,2}, Collins N. Ateba³ and Omolola E. Fayemi^{1,2*} 

Abstract

This study aimed to compare the spectroscopy, morphological, electrocatalytic properties, and antibacterial activities of cobalt nanoparticles (CoNPs) with nickel nanoparticles (NiNPs). Cobalt nanoparticles and NiNPs were prepared via a chemical reduction approach and characterized utilizing transmission electron microscopy (TEM), energy-dispersive X-ray (EDX), and X-ray diffraction (XRD) techniques. The result from XRD and TEM analysis revealed that the synthesized nanoparticles exhibit face-centered cubic with smooth spherical shape, having average particles size of 12 nm (NiNPs) and 18 nm (CoNPs). The electrochemical properties of the nanoparticles were examined via cyclic voltammetry (CV) and electrochemical impedance spectroscopy (EIS) techniques. The CV results showed that GCE-Ni (35.6 μA) has a higher current response compared to GCE-Co (10.5 μA). The EIS analysis revealed that GCE-Ni (1.39 $\text{K}\Omega$) has faster electron transport capability compared to GCE-Co (2.99 $\text{K}\Omega$) as indicated in their R_{ct} values. The power density of the synthesized nanoparticles was obtained from their "knee" frequency (f°) values, with GCE-Ni (3.16 Hz) having higher f° values compared to GCE-Co (2.00 Hz). The antibacterial activity of the nanoparticles was evaluated against multidrug-resistant *Escherichia coli* O157, *Escherichia coli* O177, *Salmonella enterica*, *Staphylococcus aureus*, and *Vibrio cholerae*. The result from the antibacterial study revealed that at low concentrations both CoNPs and NiNPs have significant antibacterial activities against *E. coli* O157, *E. coli* O177, *S. enterica*, *S. aureus*, and *V. cholerae*. NiNPs showed better antibacterial activities at low concentrations of 61.5, 61.5, 125, 61.5, and 125 $\mu\text{g/mL}$ compared to CoNPs with minimum inhibitory concentrations of 125, 125, 250, 61.5, and 125 $\mu\text{g/mL}$ against *E. coli* O157, *E. coli* O177, *S. enterica*, *S. aureus*, and *V. cholerae*, respectively. These promising antibacterial activities emphasize the potential of CoNPs and NiNPs as effective antibacterial agents, which could aid in the development of novel antibacterial medicines.

Keywords Cobalt nanoparticles, Nickel nanoparticles, Spectroscopy, Morphology, Antibacterial activities

*Correspondence:
Omolola E. Fayemi
Omolola.Fayemi@nwu.ac.za
Full list of author information is available at the end of the article

Introduction

The high mortality and morbidity resulting from disease outbreak cases worldwide is associated with the increasing incidence of antibiotic resistance among pathogens (Hofer 2019). As a result, the quest to synthesize metal nanoparticles as an alternative approach to combat pathogens becomes necessary. Metal-based nanoparticles with novel antibacterial properties are potentially promising areas for overcoming the limitations of antibiotics and resistant spread (Breijyeh et al. 2020; Abolarinwa et al. 2022; Ajose et al. 2022). Nanoparticles and nanomaterials are gaining prominence in the field of medicine owing to their diminutive size and large surface area-to-volume ratio (Rashidi Ranjbar et al. 2020; Saidin et al. 2021). Metal nanoparticles have drawn increasing attention for their possible antibacterial activities owing to their distinct physicochemical properties (Abolarinwa et al. 2022). Transition metal nanoparticles, for example, have been widely researched for their prospective applications in electronics, catalysis, and biomedical sciences (Dutta et al. 2020). Nickel nanoparticles and CoNPs have gained special interest due to their remarkable catalytic and magnetic capabilities (Tian et al. 2016).

Synthesis methods are critical in identifying nanoparticle physicochemical characteristics. Nanoparticle characterization is crucial in comprehending their chemical and physical properties, which can influence their biological activities. Cobalt nanoparticles are renowned for their high melting point, oxidation resistance, and magnetic properties. They are frequently utilized in energy storage devices, biological imaging, catalysis, and magnetic data storage, such as hard disk drives (Barakat et al. 2009). On the other hand, NiNPs possess high conductivity with outstanding mechanical properties, making them suitable for catalytic, sensor, and electronic applications. They are also used in magnetic data storage and manufacture of rechargeable batteries, such as nickel–cadmium and nickel–metal hydride batteries (Calandra 2009). In biomedical applications, both CoNPs and NiNPs have shown potential for use in drug delivery, imaging, and cancer therapy (Gupta et al. 2007).

Cobalt nanoparticles and NiNPs have been found to possess antibacterial properties, which make them attractive for use in medical and industrial applications. Research studies have shown that these nanoparticles can effectively inhibit the growth and proliferation of bacteria of several types, encompassing Gram-positive and Gram-negative ones (Fazal et al. 2022; Harish et al. 2022; Sarian et al. 2022; Hassan Afandy et al. 2023). The antibacterial properties of these nanoparticles are thought to be due to their ability to generate reactive oxygen species (ROS) that can damage bacterial cell membranes and inhibit bacterial growth (Saravanan

et al. 2021). Additionally, the small size of the nanoparticles allows them to penetrate bacterial cells more easily, leading to increased antibacterial activity (Sun et al. 2021). Furthermore, nanoparticles with smaller particle sizes have shown good antibacterial activity (Azam et al. 2012). The investigation of the antibacterial efficacy of nanoparticles was extensively researched using human pathogenic microorganisms such as *E. coli* (Al-Nabulsi et al. 2020; Xiao et al. 2021) and *S. aureus* (Attallah et al. 2022; Shaaban et al. 2023). Moreover, these microbes seem highly sensitive to transition metal nanoparticles (Yang et al. 2021; Jeevanandam et al. 2022).

Several metal oxide nanoparticles have been reported for their potential antibacterial activities against Gram-negative and Gram-positive bacteria, consisting of *Klebsiella pneumoniae*, *Escherichia coli*, *Pseudomonas aeruginosa*, and *Staphylococcus aureus*. These metal oxide nanoparticles include Al₂O₃ (Jawad et al. 2021; Karimi et al. 2021), CuO, Cu₂O, ZnO (Asamoah et al. 2020; Karuppanan et al. 2021; Han et al. 2022; Khosravi et al. 2022), CaO (Abbas and Aadim 2022), MnO₂, MgO (Ogunyemi et al. 2020; Amrulloh et al. 2021), TiO₂ (Wang et al. 2020; Zhang et al. 2021), Fe₃O₄ (Azizabadi et al. 2021; Kamali et al. 2022), Ag₂O (Rashidi Ranjbar et al. 2020; Dharmaraj et al. 2021; Mahlambi and Moloto 2022), NiO (Kannan et al. 2020; Christy et al. 2021), and SiO₂ (Attallah et al. 2022; Tran et al. 2023). The antibacterial activity lies in its physical and chemical properties, which include morphology, chemical composition, particle size, surface characteristics, solubility, crystallinity, aggregation, and crystal phase. The activity is also affected by the experimental conditions, nanoparticle concentration as well as type and number of bacteria. The pores within the bacterial external cellular membranes exhibit dimensions on the nanometer scale, while the size of bacterial cells is in the micrometer range. Since nanoparticles can be smaller than bacterial pores, they can permeate the cell membrane in a novel way (Abolarinwa et al. 2022). Preparing metal nanoparticles that are stable enough to effectively inhibit bacterial growth while in a nutrient medium is a serious issue.

Going through the literature, minimal information is available on the antibacterial properties of CoNPs and NiNPs. Realizing the potential antibacterial applications of these transition metal nanoparticles, we thereby synthesized CoNPs and NiNPs using a chemical reduction approach, examined their electrochemical properties via CV and EIS techniques, and then verified their antibacterial activities against *Escherichia coli* O157, *Escherichia coli* O177, *Salmonella enterica*, *Staphylococcus aureus*, and *Vibrio cholerae*. Additionally, the antibacterial activities of these metal nanoparticles were compared, as these

properties are essential for their prospective usage in a variety of biomedical applications.

Materials, reagents, and instruments

Cobalt acetate tetrahydrate, potassium hexacyanoferrate IV ($K_4(Fe(CN)_6)$), sodium borohydride, *N,N*-dimethyl formamide (DMF), ethylene glycol, sodium dihydrogen phosphate (NaH_2PO_4), potassium hexacyanoferrate III ($K_3(Fe(CN)_6)$), disodium hydrogen phosphate (Na_2HPO_4) were procured from Sigma-Aldrich, a reputable supplier based in Darmstadt, Germany. Ethanol, hydrochloric acid (HCl), hydrazine hydrate, sulfuric acid, sodium hydroxide (NaOH), and nickel chloride were sourced from Glass-world Chemicals, a company based in Johannesburg, South Africa. Every reagent was of high analytical grade.

Various techniques were employed to analyze the morphology and structure of the nanoparticles that were produced. Energy diffraction X-ray (EDX) analysis was performed utilizing a JEOL JSM-6610 LV equipment from Dearborn, USA. The UV-visible spectrophotometry analysis was conducted with a Cary 300 series UV-visible spectrometer sourced from Agilent Technology, based in Darmstadt, Germany. X-ray diffraction (XRD) analysis was performed utilizing instrumentation provided by Bruker Company, headquartered in Karlsruhe, Germany. The transmission electron microscopy (TEM) analysis was conducted employing a JEOL2100 instrument that was equipped with a LaB 6 electron gun manufactured by JEOL Ltd, based in Tokyo, Japan.

An electrochemical investigation involving cyclic voltammetry (CV) and impedance spectroscopy (EIS) was performed using an Autolab Potentiostat PGSTAT 302, manufactured by Eco Chemie in Utrecht, the Netherlands. The experimental setup was controlled by GPES software (version 4.9) and NOVA 2.1.3 software with FRA 32 module, which allowed for a frequency range spanning from 100 kHz to 0.1 Hz. Distilled water was used while carrying out all the experiments.

Cobalt and nickel nanoparticles synthesis

Cobalt nanoparticles were chemically synthesized via the dissolution of 2.0 g of cobalt acetate tetrahydrate in a solution comprising 2 mL of water and 8 mL of ethanol, followed by a 15-min stirring period. Next, under continuous agitation, a 5.0 mL volume of a sodium borohydride solution with a concentration of 1.08 M was gradually introduced into the amalgamation at a rate of 2 drops per second. This process continued until the formation of a greyish-black precipitate occurred. The greyish-black particles were gently collected using a magnet from the mixture and subjected to multiple washes with distilled water and ethanol. Subsequently, the particles were dried at room temperature for 24 h (Cruz et al. 2019a).

The production of NiNPs was accomplished by introducing 8 mL of a 1 M sodium hydroxide (NaOH) solution into an 800 mL ethylene glycol comprising a combination of 2 g nickel chloride and 10 mL hydrazine hydrate. The reaction mixture within a sealed container underwent continuous agitation for a duration of 45 min at a temperature of 70 °C. The black particles obtained were subjected to a meticulous cleaning process using ethanol (100%). Subsequently, the particles were sealed under vacuum conditions at a temperature of 27 °C for a duration of 24 h (Wu et al. 2012).

Glassy carbon electrode (GCE) modification procedure

The bare GCE undergoes a preliminary electrode treatment before being modified with the prepared nanoparticles. This was done by rubbing its surface on a Sic Emery pad soaked with aluminum oxide paste. Afterward, enough distilled water was used to rinse the GCE to eliminate any leftover aluminum oxide particles. To achieve thorough cleaning, the GCE was ultrasonicated for about 5 min in a container containing distilled water, followed by another 5 min in methanol. Each of the nanoparticle pastes was applied to the cleaned GCE surface via a drop-casting method. The cleaned GCE was modified with about 5 μ L of the prepared CoNPs and NiNPs using drop-dry method, for about 5 min at 50 °C in the oven. The coated electrodes were designated as GCE-Co and GCE-Ni.

Antimicrobial assay of the nickel and cobalt nanoparticles

The bacterial isolates

Five pathogenic bacteria (*Escherichia coli* O157, *Escherichia coli* O177, *Salmonella enterica*, *Staphylococcus aureus*, and *Vibrio cholerae*) were obtained from the Antimicrobial Resistance and Phage Biocontrol Laboratory, Department of Microbiology, North-West University (Mafikeng Campus), South Africa. The bacteria had been confirmed to be multi-drug resistant, and details on the bacteria source, virulence, and multi-drug resistance profiles are described in Table 1.

Preparation of bacteria culture

Before NPs antimicrobial test, the isolates were revived by cultured in nutrient broth and subjected to incubation at a temperature of 37 °C for a duration of 24 h. The absorbance of the bacterial cultures was standardized using a spectrophotometer (MB-580 model, Shenzhen Huisong Technology Development Co., Ltd., Shenzhen, China) to achieve a standardized value of 0.5 on the MacFarland Standard scale.

Table 1 Virulence and antibiotics resistance profile of the bacteria sample

| Bacteria | Source | Virulence gene | Antibiotics resistance profile |
|---------------------|---------------|--|--|
| <i>E. coli</i> O156 | Cattle faeces | β -D-glucuronidase gene (<i>uidA</i>), Shiga toxin 1 (<i>stx1</i>), Shiga toxin 2 (<i>stx2</i>), Intimin gene (<i>eae</i>) | Azithromycin, Rifamycin, Penicillin, Ampicillin, Sulfamethoxazole, Tetracycline |
| <i>E. coli</i> O177 | Cattle faeces | β -D-glucuronidase gene (<i>uidA</i>), Heat-stable toxin (<i>St</i>), Heat-labile toxin (<i>lt</i>), Intimin gene (<i>eae</i>) | Azithromycin, Rifamycin, Penicillin, Ampicillin, Sulfamethoxazole |
| <i>S. Enterica</i> | Cattle faeces | Invasion gene (<i>InvA</i>), <i>Salmonella</i> plasmid virulence (<i>sop</i>) | Norfloxacin, Ampicillin, Azithromycin, Rifamycin, Penicillin, Tetracycline, Sulfamethoxazole |
| <i>V. cholerae</i> | Cattle faeces | <i>V. cholerae</i> (<i>v. cholera</i>), Accessory cholera enterotoxin (<i>ace</i>), cholera toxin (<i>ctxA</i>) | Azithromycin, Rifamycin, Penicillin, Ampicillin, Sulfamethoxazole, Tetracycline |
| <i>S. aureus</i> | Milk | Staphylococcal enterotoxin A (<i>sea</i>), nuclease (<i>Nuc</i>) | Azithromycin, Rifamycin, Penicillin, Ampicillin, Tetracycline |

Nanoparticles preparation for antibacterial test

Before the NPs antimicrobial test, the NPs were heated for aim of sterilization in an oven for 2 h. Thereafter, NPs suspension (1000 $\mu\text{g}/\text{mL}$) was prepared by adding 1000 μg of each NPs to 1 mL of an organic solvent, dimethyl sulfoxide (DMSO). The mixture was sonicated for few minutes to form a solution.

Antibacterial activity of nickel and cobalt nanoparticles

The bacteria's susceptibility to the NPs was examined via disc diffusion technique. First, freshly prepared Mueller–Hinton Agar (MHA) was inoculated with a standardized bacteria culture. Thereafter, sterilized paper disc soaked in NPs solution was placed aseptically on inoculated MHA and incubated at a temperature of 37 $^{\circ}\text{C}$ for a duration of 24 h. The paper disc containing DMSO was adopted as control. The zones of inhibition were observed and measured in millimeter. The experiments were performed in triplicate.

Minimum inhibitory concentration of nickel and cobalt nanoparticles

The minimum inhibitory concentration (MIC) of the NPs was evaluated utilizing 96-microplate broth dilution method. Firstly, all the microtiter plate wells marked for the experiments were filled with 100 μL of sterile double-strength nutrient broth. Exactly, 100 μL of the NPs (1000 $\mu\text{g}/\text{mL}$) solution was added to the first well and dilution was carried out to obtain various concentrations (31.25, 62.5, 125, 250, and 500 $\mu\text{g}/\text{mL}$) of the nanoparticles. Thereafter, a 10 μL of the standardized bacteria was aseptically dispensed to each well and incubated at 37 $^{\circ}\text{C}$. Immediately (at 0 h) and after 24 h, the optical density (OD) of the suspension in the microtiter plates was measured using a microplate reader at 630 nm. The DMSO was used as solvent control. The experiments were performed in triplicate. The MIC of NPs was taken as the lowest concentration of the NPs where its OD at 24 h was equal to OD at 0 h.

Minimum bactericidal concentration of nickel and cobalt nanoparticles

The minimum bactericidal concentration (MBC) of the NPs against the bacterial pathogens was determined from MIC experiment. Immediately the MIC was determined, and the wells that contained suspension of MIC and above concentration were marked. Exactly 100 μL of the suspension from each marked well was withdrawn and mixed with nutrient agar at 45 $^{\circ}\text{C}$ and pour into Petri dish plate. Thereafter, the plates underwent incubation for 24 h at 37 $^{\circ}\text{C}$ and observed for colony formation. The MBC was taken as the minimum concentration of NPs at which no visible colony was observed.

Results and discussion

Energy-dispersive X-ray analysis

Energy-dispersive X-ray is a useful technique for analyzing the elemental composition of nanoparticles, as it is non-destructive and can provide information about the composition of the sample at the nanoscale. The elemental composition of CoNPs and NiNPs is given by their EDX spectra depicted in Fig. 1. The existence of a small percentage of carbon, sodium, and oxygen in Fig. 1a (CoNPs spectrum) is intruded impurities from the precursors, ditto to Fig. 1b (NiNPs spectrum) where the carbon and oxygen were also impurities from the precursors.

X-ray diffraction analysis

The crystalline structures of the synthesized CoNPs and NiNPs were examined via XRD. As shown in the XRD diffractograms, both CoNPs and NiNPs (Fig. 2) exhibit three major diffraction peaks each. Cobalt nanoparticles have its diffraction peaks at 2θ of 44.7 $^{\circ}$ (1 1 1), 52.0 $^{\circ}$ (2 0 0), and 76.3 $^{\circ}$ (2 2 0), which correspond to the face-centered cubic (FCC) crystal structure of pure CoNPs. The diffraction peaks observed exhibit a resemblance to those documented in the literature for CoNPs (Khusnuriylova et al. 2021; Shi et al. 2021; Cruz et al. 2019b), thereby confirming the accomplished synthesis of pure CoNPs in the FCC

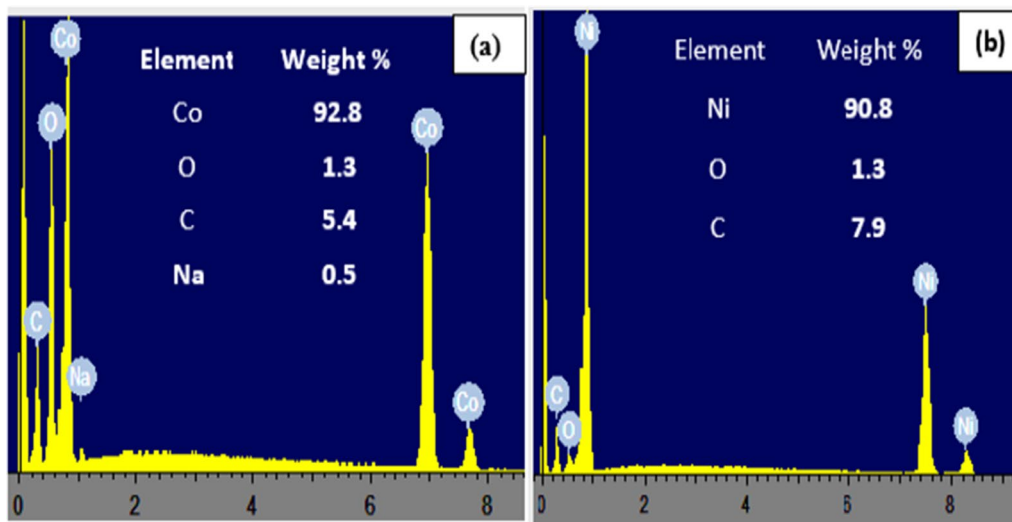


Fig. 1 EDX spectra of **a** CoNPs and **b** NiNPs

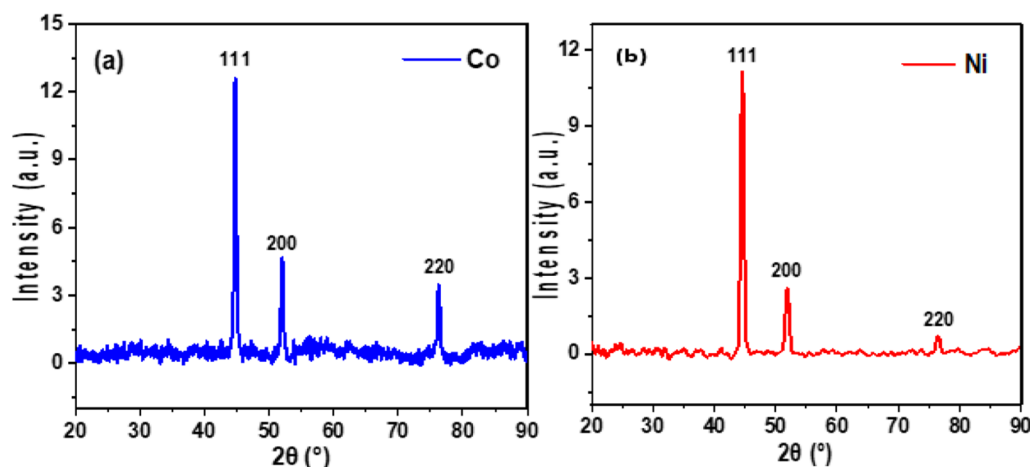


Fig. 2 XRD spectra of **a** CoNPs and **b** NiNPs

structure. The diffraction peaks of NiNPs can be observed at 2θ which is equal to 44.5° (1 1 1), 51.9° (2 0 0), and 76.5° (2 2 0), indicating the presence of an FCC crystal structure in the pure NiNPs.

The diffraction peaks observed exhibit a resemblance to the ones documented in the literature for NiNPs (Wu et al. 2012, 2010; Eluri and Paul 2012; Balogun and Fayemi 2023), thereby confirming the successful formation of FCC pure NiNPs. Applying Scherrer's equation (Monshi et al. 2012), 12 nm and 18 nm were obtained as average crystallite size (L) for NiNPs and CoNPs, respectively, as given in Eq. 1.

$$L = \frac{0.89\lambda}{B \cos \theta} \quad (1)$$

In this context, θ denotes the Bragg angle of the X-ray diffraction, λ designates the wavelength (0.15418 nm), and B stands for full-width half-maximum.

Transmission electron microscopy

The prepared nanoparticles' sizes and shapes were identified utilizing transmission electron microscopy. Figure 3a, b displays the TEM images of CoNPs and NiNPs, respectively. The TEM image of CoNPs as depicted in Fig. 3a, displays a spherical particle shape with an irregular particle morphology. The average particle size is measured to be 17.4 nm, which closely aligns with the value calculated using Scherrer's equation. The NiNPs, conversely, show a spherical particle configuration with a uniform particle morphology, possessing an average

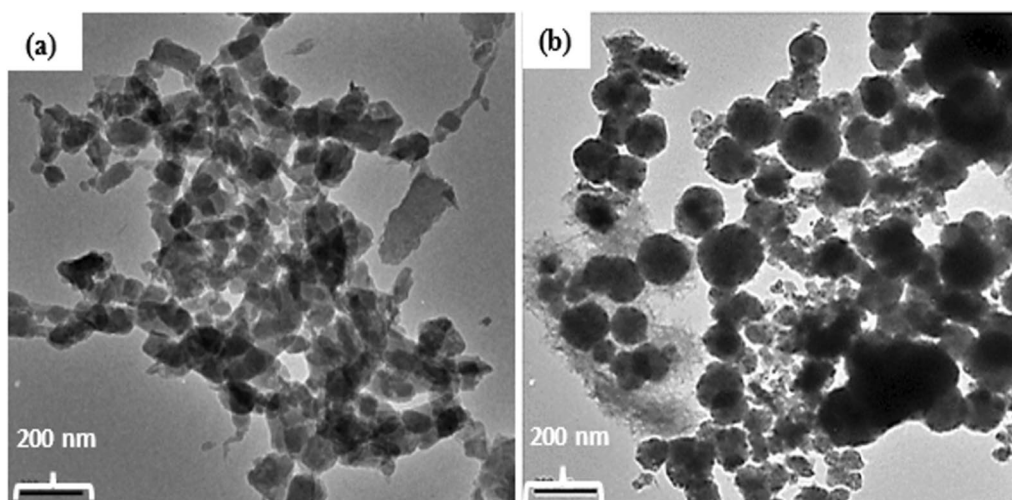


Fig. 3 TEM images of **a** CoNPs and **b** NiNPs

particle size of 11.7 nm, akin to the outcome derived from the utilization of Scherrer's equation for the NiNPs.

Ultraviolet–visible analysis

The UV–visible spectra for CoNPs and NiNPs are illustrated in Figure 4. Cobalt nanoparticles exhibit an absorption peak at 291 nm and a broad absorption peak from 385 to 510 nm (Figure 4a, b). The peaks can be assigned to the $O^{2-} \rightarrow Co^{2+}$ and $O^{2-} \rightarrow Co^{3+}$ charge transfer process (Adekunle et al. 2020). Similarly, NiNPs have an absorption peak at 293 nm. The absorption peaks that were observed bear similarities to those reported in the literature concerning NiNPs and CoNPs (Bathla and Pal 2018; Moumen et al. 2019; Balogun and Fayemi 2024).

Interestingly, the absorption peaks of the two nanoparticles are close to each other.

Electrochemical studies

Cyclic voltammetry

All electrodes were electrochemically characterized using cyclic voltammetry (CV) to evaluate the nanoparticles' electron transport behaviors. As seen in the cyclic voltammograms (Fig. 5), all of the electrodes exhibited a pair of redox peaks in 5 mM $K_3/K_4(Fe(CN)_6)$ produced in a solution of 0.1 M PBS at a pH of 7. The electrodes' peak separations (E_p) values for GCE, GCE-Co, and GCE-Ni were (0.39 V), (0.50 V), and (0.18 V), respectively, as seen in Table 2. The obtained E_p values are more than

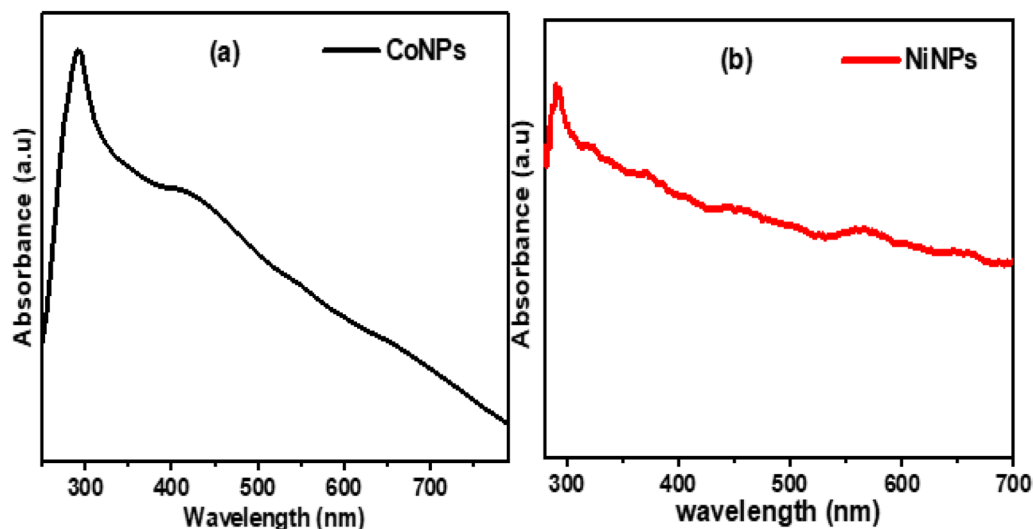


Fig. 4 UV–visible spectra of **a** CoNPs and **b** NiNPs

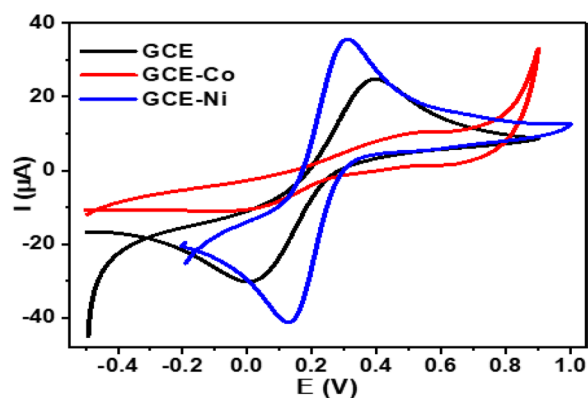


Fig. 5 Cyclic voltammograms of the electrodes in 5 mM $K_3/K_4(Fe(CN)_6)$ produced in 0.1 M of PBS at 25 mV s^{-1}

the predicted 0.059 V for quick one-electron transportation, demonstrating a quasi-reversible mechanism at the electrode interfaces (Haque et al. 2013; Zangeneh Kamali et al. 2014). All electrode's I_{pa}/I_{pc} values are nearly equal to one, as shown further in Table 2, which indicates reversibility at all the electrodes. As depicted in Fig. 5, GCE-Ni (35.6 μA) has a higher current response compared to GCE-Co (10.5 μA). The anodic peak current (I_{pa}) obtained for the GCE-Ni is thrice compared to GCE-Co. This implies that among the electrodes, the GCE-Ni has the best current response. The electrochemical properties of these electrodes were further assessed via EIS analysis.

Scan rate study

The scan rate study focused on analyzing the impact of altering the scan rate (ranging from 25 to 300 mV s^{-1}) on the electrochemical phenomena occurring at the surface of the electrode. The experiment utilized a solution containing 5 mM of $K_3/K_4(Fe(CN)_6)$ in a PBS solution of 0.1 M. As depicted in Fig. 6a, b, increasing in the scan rate exhibits a direct correlation an increase in the peak currents. The relationship between the square root of the scan rate and the peak current displayed in Fig. 6x and y, gives a linearity, with the following regression Eqs. (2–5):

$$\text{For CoNPs: } I_{pa} = 0.0001v^{1/2}8.0928E - 6 \quad (R^2 = 0.9856) \quad (2)$$

$$I_{pc} = -6.5950E - 5v^{1/2} - 8.6212E - 6 \quad (R^2 = 0.9356) \quad (3)$$

$$\text{For NiNPs: } I_{pa} = 2.7546E - 4v^{1/2}3.5663E - 5 \quad (R^2 = 0.9932) \quad (4)$$

$$I_{pc} = -2.256E - 4v^{1/2} - 4.4876E - 5 \quad (R^2 = 0.9921) \quad (5)$$

A diffusion-controlled process is therefore suggested for both GCE-Co and GCE-Ni based on the linear relationship existing between the peak currents and the scan rate's square root.

Stability study

Both GCE-Co and GCE-Ni were subjected to stability tests using CV with 50 mVs^{-1} for 20 repetitive scans in 5 mM of $K_3/K_4(Fe(CN)_6)$ in a PBS solution of 0.1 M. According to Fig. 7a, b, a small current drop of 7.4% and 4.5% was recorded for GCE-Co and GCE-Ni, respectively, implying a high stability of both electrodes. Going by this result, GCE-Ni (95.5%) is more stable than GCE-Co (92.6%).

Electrochemical impedance spectroscopy (EIS) study

An EIS investigation was conducted in 5 mM of $K_3/K_4(Fe(CN)_6)$ made in a PBS solution of 0.1 M (pH 7) to thoroughly examine the electron transport behaviors of these electrodes. The operating parameters include 0.3 V, Ag/AgCl, 3 M KCl (saturated), and 100 kHz–0.1 Hz. Figure 8 shows the Nyquist plots of the electrodes' EIS fitted data with an inset representing the equivalent circuit used to fit the EIS data. As seen in the electrochemical circuit, CPE designates constant phase element, W connotes Warburg impedance, R_{ct} represents charge transfer resistance, while R_s stands for solution resistance.

The fitted EIS data and individual Chi-square (χ^2) values are provided in Table 3. The negative Chi-square values and the small % errors obtained, imply that the EIS data were accurately fitted. Table 3 presents the R_{ct} values of the electrodes as 1.39, 2.99, and 8.73 $\text{K}\Omega$ for GCE-Ni, GCE-Co, and GCE, respectively. It is observed that GCE-Ni exhibits the lowest R_{ct} , therefore having a faster ability to transport electrons than Co-GCE. The observed

Table 2 Cyclic voltammetry data obtained for the electrodes

| Electrode | I_{pa} (μA) | I_{pc} (μA) | I_{pa}/I_{pc} | E_{pa} (V) | E_{pc} (V) | ΔE_p (V) | E° (V) |
|-----------|----------------------------|----------------------------|-----------------|--------------|--------------|------------------|---------------|
| GCE | 25.0 | -30.0 | -0.83 | 0.40 | 0.01 | 0.39 | 0.20 |
| GCE-Co | 10.5 | -10.5 | -1.00 | 0.51 | 0.01 | 0.50 | 0.25 |
| GCE-Ni | 35.6 | -41.3 | -0.86 | 0.31 | 0.13 | 0.18 | 0.09 |

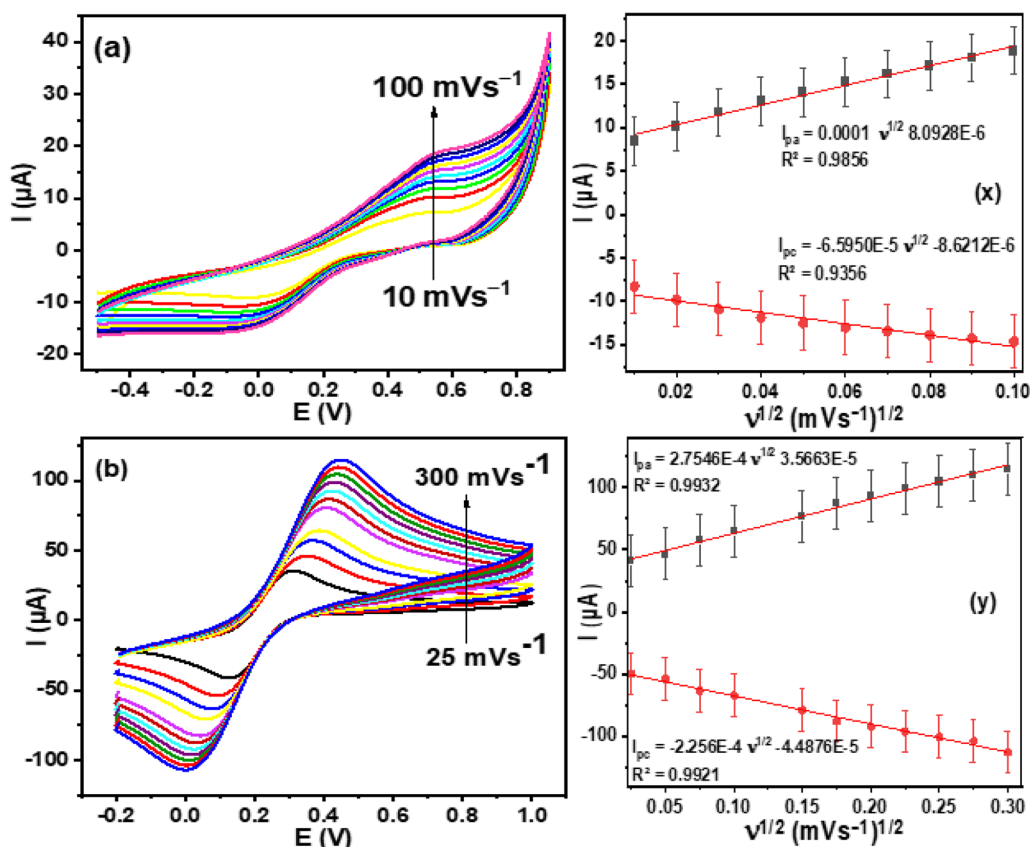


Fig. 6 Cyclic voltammogram of **a** GCE-Co and **b** GCE-Ni from 10 to 100 mVs^{-1} and 25–300 mVs^{-1} , respectively, 5 mM of $\text{K}_3/\text{K}_4(\text{Fe}(\text{CN})_6)$ in a PBS solution of 0.1 M, and (x) and (y) linear plots of peak current vs scan rate's square root

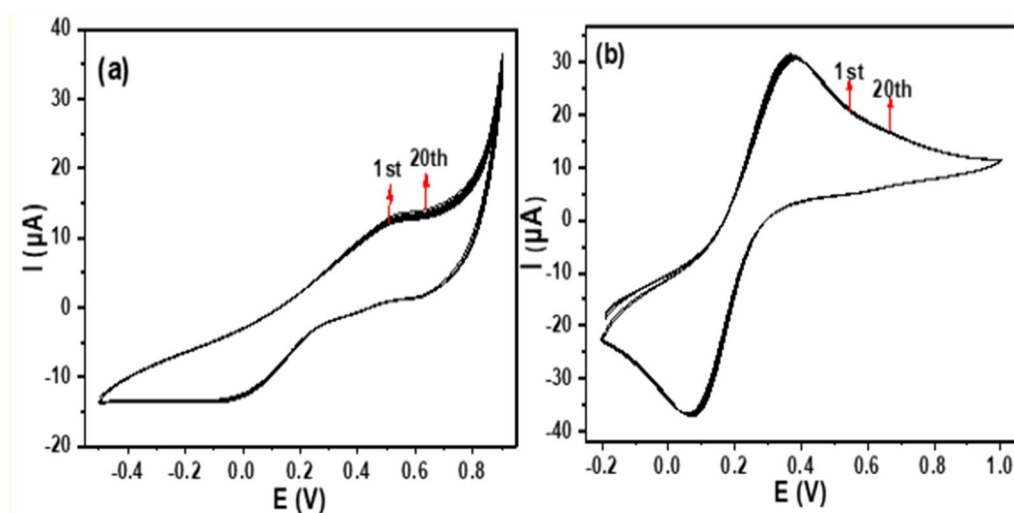


Fig. 7 Cyclic voltammograms of **a** GCE-Co and **b** GCE-Ni with 20 scans at 25 mVs^{-1} in 5 mM of $\text{K}_3/\text{K}_4(\text{Fe}(\text{CN})_6)$ made in a PBS solution of 0.1 M

decrease in R_{ct} values of the treated electrodes indicates successful coating of the nanoparticles on the bare electrode. The EIS result exhibits a resemblance to the one

obtained for CV except for CoNPs. The electrode n values (0.72–0.86) might also account for the ease at which ions diffuse between the solution and electrode.

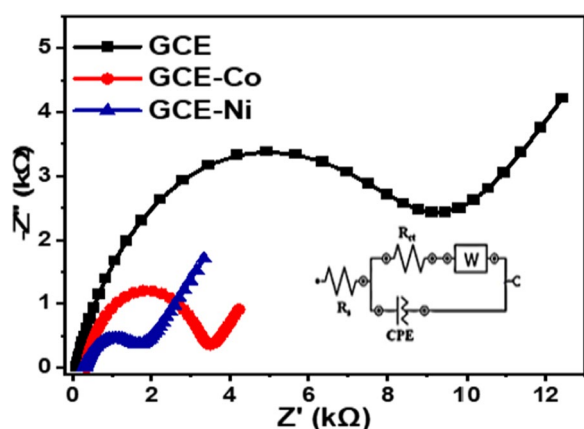


Fig. 8 Nyquist plots of the electrodes in 5 mM of $K_3/K_4(Fe(CN)_6)$ made in a PBS solution of 0.1 M (pH 7), and inset represents the equivalent circuit employed to fit the obtained EIS data

The determination of the "knee" frequency (f^o) of the electrodes was conducted in order to get deeper insights into the electronic characteristics of the electrodes. This frequency plays a crucial role in determining the power density, which refers to the supercapacitor's charge and discharge capability. A supercapacitor with a greater f^o has a quicker charge and discharge capacity, thus a better power density (Du and Pan 2006; Huang et al. 2007; Balogun and Fayemi 2022). The following f^o values 3.16, 2.00, and 1.68 Hz were recorded for the GCE-Ni, GCE-Co, and GCE, respectively. This result indicates that GCE-Co has a lower f^o value compared to GCE-Ni. However, the two modified electrodes (GCE-Co and GCE-Ni) are far better than the uncoated electrodes. The large f^o value of GCE-Ni corroborates its high electron transport capability. In accordance with a study (Adekunle et al. 2013), the preponderance of commercially accessible supercapacitors, notably those designed for higher power applications, run at frequencies below 1 Hz.

Antibacterial study

Antimicrobial activities of nickel and cobalt nanoparticles

In this study, both NiNPs and CoNPs displayed antibacterial properties against the *E. coli* O157, *E. coli* O177, *S. enterica*, *S. aureus*, and *V. cholerae* tested (Fig. 9). Similar

antibacterial activities have been reported by several researchers for NPs (Abbas and Aadim 2022; Aghari et al. 2020; Betsy et al. 2022). Aghari et al. (Aghari et al. 2020) reported antibacterial activities of NiNPs against *Staphylococcus aureus* and *Escherichia coli*. Also, study by Abass et al. (Abass et al. 2021) indicates that NPs had bactericidal activity against multidrug-resistant bacteria.

Nanoparticles minimum inhibitory concentration (MIC)

The (MIC) of NPs against tested bacterial pathogens varies. It was observed that the NiNPs had better inhibitory activities against *E. coli* O157, *E. coli* O177, *S. enterica*, *S. aureus*, and *V. cholerae*, with MIC values of 61.5, 61.5, 125, 61.5, and 125 $\mu\text{g/mL}$ compared to CoNPs MIC values of 125, 125, 250, 61.5, and 125 $\mu\text{g/mL}$, respectively. Both NiNPs and CoNPs show lower inhibitory concentration value (61.5 $\mu\text{g/mL}$) against *V. cholerae* (Table 4). In contrast, NiNPs and CoNPs show higher inhibitory concentration value (125 and 250 $\mu\text{g/mL}$) against *S. enterica*. The variation in antimicrobial activities of the NPs might be explained from several parameters including size, charge, chemical makeup, and agglomeration state of the NPs (Abolarinwa et al. 2022).

Minimum bactericidal concentration of the nanoparticles

In this study, NiNPs had better bactericidal activities against *E. coli* O157, *E. coli* O177, *S. enterica*, *S. aureus*, and *V. cholerae* tested compared to CoNPs. The MBC values of NiNPs against *E. coli* O157, *E. coli* O177, *S. enterica*, *S. aureus*, and *V. cholerae* were 500, 250, 250, 125, and 125 $\mu\text{g/mL}$, respectively (Fig. 10). In contrast, CoNPs had MBC values of 500, 500, 250, 250, and 250 $\mu\text{g/mL}$ against *E. coli* O157, *E. coli* O177, *S. enterica*, *S. aureus*, and *V. cholerae*, respectively (Fig. 11).

Conclusion

In this study, we synthesized CoNPs and NiNPs via a chemical reduction approach and characterized them using FTIR, TEM, EDX, and XRD techniques. The result from XRD and TEM analysis revealed that the NiNPs was smaller (12 nm) in size compared to CoNPs (18 nm). The electrochemical properties of the nanoparticles were evaluated using CV and EIS analysis, demonstrating the

Table 3 Overview of the EIS results

| Electrode | R_{ct} (Ω) | R_s (Ω) | W (F) | CPE (μF) | N | χ^2 | f^o |
|--------------------------------------|-----------------------|--------------------|------------|-----------------------|-------------|----------|-------|
| Impedance Data (% errors in bracket) | | | | | | | |
| GCE | 8.73 (5.31) | 110 (3.78) | 226 (1.84) | 3.80 (16.7) | 0.80 (1.26) | 0.555 | 1.68 |
| GCE-Co | 2.99 (2.02) | 349 (1.59) | 995 (10.9) | 2.07 (10.1) | 0.86 (1.59) | 0.204 | 2.00 |
| GCE-Ni | 1.39 (3.43) | 301 (2.03) | 524 (4.46) | 6.70 (16.3) | 0.72 (2.91) | 0.215 | 3.16 |

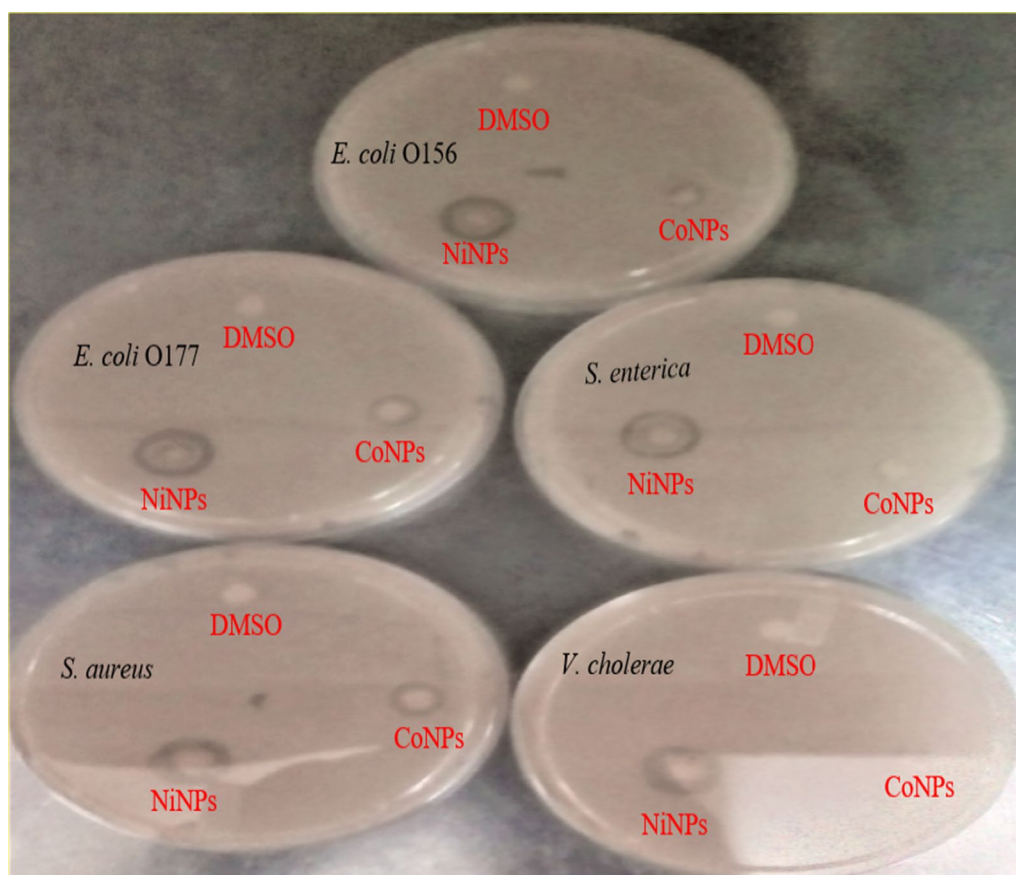


Fig. 9 Antibacterial activities of CoNPs and NiNPs against the tested bacteria pathogens

Table 4 The minimum inhibitory concentration of NiNPs and CoNPs against bacteria isolates

| Bacteria | NiNPs | CoNPs |
|--|-------|-------|
| <i>Minimum inhibitory concentration of NPs (μg/mL)</i> | | |
| <i>E. coli</i> O156 | 61.5 | 125 |
| <i>E. coli</i> O177 | 61.5 | 125 |
| <i>S. Enterica</i> | 125 | 250 |
| <i>V. cholerae</i> | 61.5 | 61.5 |
| <i>S. aureus</i> | 125 | 250 |

superiority of GCE-Ni with a higher current response of 35.6 μA over to GCE-Co (10.5 μA). The EIS studies indicated that GCE-Ni (1.39 $\text{K}\Omega$) has superior electron transport capability compared to GCE-Co (2.99 $\text{K}\Omega$) due to its lower R_{ct} values. Furthermore, the power density of the

synthesized nanoparticles was determined based on their "knee" frequency (f^*) values. The GCE-Ni (3.16 Hz) exhibited a greater f^* value compared to GCE-Co (2.00 Hz). Interestingly, both NiNPs and CoNPs possessed significant antibacterial activities against *E. coli* O157, *E. coli* O177, *S. enterica*, *S. aureus*, and *V. cholerae*, possibly due to their size, electrical, and optical properties. Here, NiNPs displayed a higher antibacterial potential compared to CoNPs. Its smaller particle size and faster electron transport significantly influenced its performance among other properties by providing a larger specific surface area, an increased bacterial cell membrane permeability, and a higher antibacterial activity. Lastly, this research sheds light on the synthesis, characterization, and antibacterial properties of CoNPs and NiNPs, which can be used to generate novel antimicrobial drugs.

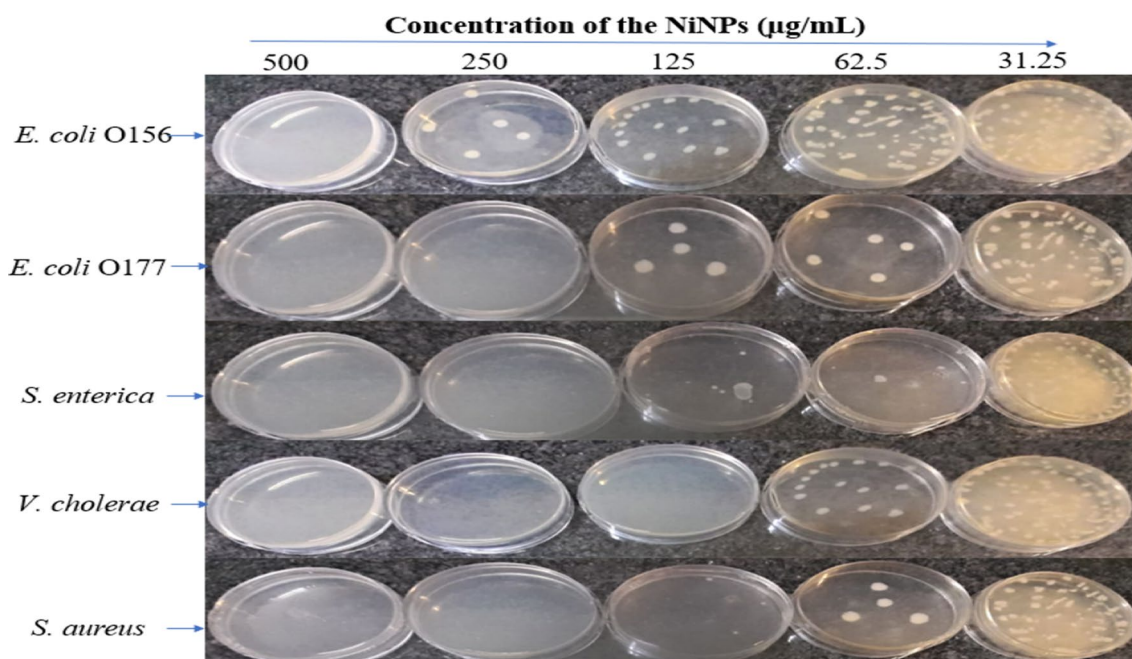


Fig. 10 The minimum bactericidal concentration exhibited by NiNPs against bacteria isolates

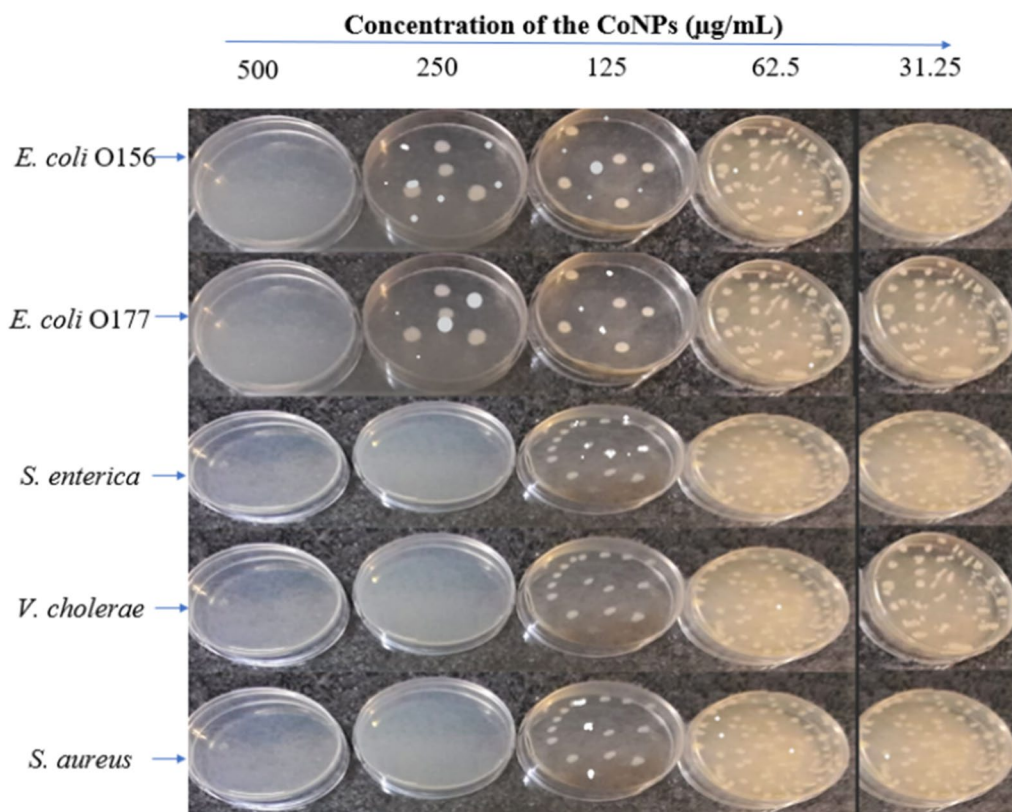


Fig. 11 The minimum bactericidal concentration exhibited by CoNPs against bacteria isolates

Abbreviations

| | |
|-------|------------------------------------|
| CoNPs | Cobalt nanoparticles |
| CV | Cyclic voltammetry |
| DMF | <i>N,N</i> -Dimethyl formamide |
| DMSO | Dimethyl sulfoxide |
| EIS | Impedance spectroscopy |
| Ep | Electrodes' peak |
| EDX | Energy-dispersive X-ray |
| FCC | Face-centered cubic |
| GCE | Glassy carbon electrode |
| MBC | Minimum bactericidal concentration |
| MHA | Mueller-Hinton Agar |
| MIC | Minimum inhibitory concentration |
| NiNPs | Nickel nanoparticles |
| NP | Nanoparticle |
| OD | Optical density |
| TEM | Transmission electron microscopy |
| XRD | X-ray diffraction |

Acknowledgements

The authors wish to appreciate the Department of Chemistry and Department of Microbiology, North-West University, South Africa.

Author contributions

OEF conceptualized and supervised the study, and OEF and CN helped in resources. SB, TA, FA, CN, and OF were involved in writing and editing. SB and TA experimented the study. All authors contributed to the article and approved the submitted version.

Funding

Open access funding provided by North-West University. We are grateful to North-West University for the financial support.

Availability of data and materials

Not applicable.

Declarations

Ethics approval and consent to participate

Not applicable.

Consent for publication

Not applicable.

Competing interests

The authors declare no conflicts of interest.

Author details

¹Department of Chemistry, School of Physical and Chemical Sciences, Faculty of Natural and Agricultural Sciences, North-West University (Mafikeng Campus), Private Bag X2046, Mmabatho 2735, South Africa. ²Material Science Innovation and Modelling (MaSIM) Research Focus Area, Faculty of Natural and Agricultural Sciences, North-West University (Mafikeng Campus), Private Bag X2046, Mmabatho 2735, South Africa. ³Antimicrobial Resistance and Phage Biocontrol Research Group, Department of Microbiology, School of Biological Sciences, Faculty of Natural and Agricultural Sciences, North-West University, Private Bag X2046, Mmabatho 2735, South Africa.

Received: 11 April 2024 Accepted: 19 May 2024

Published online: 04 June 2024

References

- Abass AA, Alaarage WK, Abdulrudha NH, Haider J. Evaluating the antibacterial effect of cobalt nanoparticles against multi-drug resistant pathogens. *J Med Life*. 2021;14(6):823. <https://doi.org/10.25122/jml-2021-0270>.
- Abbas IK, Aadim KA. Synthesis and study of structural properties of calcium oxide nanoparticles produced by laser-induced plasma and its effect on antibacterial activity. *Sci Technol Indonesia*. 2022;7(4):427–34. <https://doi.org/10.26554/sti.2022.7.4.427-434>.
- Abolarinwa TO, Ajose DJ, Oluwarinde BO, Fri J, Montso KP, Fayemi OE, et al. Plant-derived nanoparticles as alternative therapy against diarrheal pathogens in the era of antimicrobial resistance: a review. *Front Microbiol*. 2022;13:1007115. <https://doi.org/10.3389/fmicb.2022.1007115>.
- Adekunle AS, Ozoemena KI, Agboola BO. MWCNTs/metal (Ni Co, Fe) oxide nanocomposite as potential material for supercapacitors application in acidic and neutral media. *J Solid State Electrochem*. 2013;17(5):1311–20. <https://doi.org/10.1007/s10008-012-1978-y>.
- Adekunle AS, Oyekunle JAO, Durosinmi LM, Oluwafemi OS, Olayanju DS, Akinola AS, et al. Potential of cobalt and cobalt oxide nanoparticles as nanocatalyst towards dyes degradation in wastewater. *Nano-Struct Nano-Objects*. 2020;21: 100405. <https://doi.org/10.1016/j.nanoso.2019.100405>.
- Adochiye C-Ş, Viştelaru C, Parau AC, Kiss AE, Pană I, Vlădescu A, et al. Synthesis and investigation of antibacterial activity of thin films based on TiO₂-Ag and SiO₂-Ag with potential applications in medical environment. *Nanomaterials* [internet]. 2022;12(6):902.
- Aghari MR, Soltaninejad V, Maleki A. Synthesis of nickel nanoparticles by a green and convenient method as a magnetic mirror with antibacterial activities. *Sci Rep*. 2020;10(1):12627. <https://doi.org/10.1038/s41598-020-69679-4>.
- Ajose DJ, Abolarinwa TO, Oluwarinde BO, Montso PK, Fayemi OE, Aremu AO, et al. Application of plant-derived nanoparticles (PDNP) in food-producing animals as a bio-control agent against antimicrobial-resistant pathogens. *Biomedicines*. 2022;10(10):2426. <https://doi.org/10.3390/biomedicines10102426>.
- Al-Nabulsi A, Osaili T, Sawalha A, Olaimat AN, Albiss BA, Mehyar G, et al. Antimicrobial activity of chitosan coating containing ZnO nanoparticles against *E. coli* O157:H7 on the surface of white brined cheese. *Int J Food Microbiol*. 2020;334:108838. <https://doi.org/10.1016/j.ijfoodmicro.2020.108838>.
- Amrulloh H, Fatiqin A, Simanjuntak W, Afriyani H, Annisa A. Antioxidant and antibacterial activities of magnesium oxide nanoparticles prepared using aqueous extract of Moringa oleifera bark as green agents. *J Multidiscip Appl Natl Sci* 2021.
- Asamoah RB, Annan E, Mensah B, Nbelayim P, Apalangya V, Onwona-Agyeman B, et al. A comparative study of antibacterial activity of CuO/Ag and ZnO/Ag nanocomposites. *Adv Mater Sci Eng*. 2020;2020:7814324. <https://doi.org/10.1155/2020/7814324>.
- Attallah NGM, Elekhawy E, Negm WA, Hussein IA, Mokhtar FA, Al-Fakhry OM. In vivo and in vitro antimicrobial activity of biogenic silver nanoparticles against staphylococcus aureus clinical isolates. *Pharmaceuticals* [internet]. 2022;15(2):521.
- Azam A, Ahmed AS, Oves M, Khan MS, Habib SS, Memic A. Antimicrobial activity of metal oxide nanoparticles against Gram-positive and Gram-negative bacteria: a comparative study. *Int J Nanomed*. 2012;7:6003–9. <https://doi.org/10.2147/IJN.S35347>.
- Azizabadi O, Akbarzadeh F, Danshina S, Chauhan NPS, Sargazi G. An efficient ultrasonic assisted reverse micelle synthesis route for Fe₃O₄@Cu-MOF/core-shell nanostructures and its antibacterial activities. *J Solid State Chem*. 2021;294: 121897. <https://doi.org/10.1016/j.jssc.2020.121897>.
- Balogun SA, Fayemi OE. Effects of electrolytes on the electrochemical impedance properties of NiPcMWCNTs-modified glassy carbon electrode. *Nanomaterials* [internet]. 2022;12(11):1876.
- Balogun SA, Fayemi OE. Impedance and voltammetry detection of bromate in food samples using NiPcMWCNTs modified glassy carbon electrode. *J Anal Sci Technol*. 2023;14(1):30. <https://doi.org/10.1186/s40543-023-00396-z>.
- Balogun SA, Fayemi OE. Impedance and voltammetric detection of bromate in food samples using CoPcMWCNTs nanocomposites modified glassy carbon electrode. *J Electroanal Chem*. 2024;953: 118010. <https://doi.org/10.1016/j.jelechem.2023.118010>.
- Barakat NAM, Kim B, Yi C, Jo Y, Jung M-H, Chu KH, et al. Influence of cobalt nanoparticles' incorporation on the magnetic properties of the nickel nanofibers: cobalt-doped nickel nanofibers prepared by electrospinning. *J Phys Chem C*. 2009;113(45):19452–7. <https://doi.org/10.1021/jp905667s>.
- Bathla A, Pal B. Catalytic selective hydrogenation and cross coupling reaction using polyvinylpyrrolidone-capped nickel nanoparticles.

- ChemistrySelect. 2018;3(17):4738–44. <https://doi.org/10.1002/slct.201800699>.
- Bensy AD, Christobel GJ, Muthusamy K, Alfarhan A, Anantharaman PJJ. Green synthesis of iron nanoparticles from *Ulva lactuca* and bactericidal activity against enteropathogens. *J King Saud Univ-Sci*. 2022;34(3): 101888. <https://doi.org/10.1016/j.jksus.2022.101888>.
- Brejijeh Z, Jubeh B, Karaman R. Resistance of gram-negative bacteria to current antibacterial agents and approaches to resolve it. *Molecules*. 2020;25(6):1340. <https://doi.org/10.3390/molecules25061340>.
- Calandra P. Synthesis of Ni nanoparticles by reduction of NiCl₂ ionic clusters in the confined space of AOT reversed micelles. *Mater Lett*. 2009;63(28):2416–8. <https://doi.org/10.1016/j.matlet.2009.08.016>.
- Christy AJ, Suresh S, Nehru LC. Enhanced antibacterial and photocatalytic activities of nickel oxide nanostructures. *Optik*. 2021;237: 166731. <https://doi.org/10.1016/j.jijleo.2021.166731>.
- Cruz JC, Nascimento MA, Amaral HAV, Lima DSD, Teixeira APC, Lopes RP. Synthesis and characterization of cobalt nanoparticles for application in the removal of textile dye. *J Environ Manage*. 2019a;242:220–8. <https://doi.org/10.1016/j.jenvman.2019.04.059>.
- Cruz JC, Nascimento MA, Amaral HA, Lima DS, Teixeira APC, Lopes RP. Synthesis and characterization of cobalt nanoparticles for application in the removal of textile dye. *J Environ Manage*. 2019b;242:220–8.
- Dharmaraj D, Krishnamoorthy M, Rajendran K, Karuppiah K, Annamalai J, Durairaj KR, et al. Antibacterial and cytotoxicity activities of biosynthesized silver oxide (Ag₂O) nanoparticles using *Bacillus paramycooides*. *J Drug Deliv Sci Technol*. 2021;61:102111. <https://doi.org/10.1016/j.jddst.2020.102111>.
- Du C, Pan N. Supercapacitors using carbon nanotubes films by electrophoretic deposition. *J Power Sources*. 2006;160(2):1487–94. <https://doi.org/10.1016/j.jpowsour.2006.02.092>.
- Dutta RR, Devi R, Dutta HS, Gogoi S. Chapter 7: Transition metal dichalcogenides for biomedical applications. In: Khan R, Barua S, editors. *Two-Dimensional Nanostructures for Biomedical Technology*; Elsevier. 2020. p. 211–47.
- Eluri R, Paul B. Synthesis of nickel nanoparticles by hydrazine reduction: mechanistic study and continuous flow synthesis. *J Nanopart Res*. 2012;14(4):800. <https://doi.org/10.1007/s11051-012-0800-1>.
- Fazal A, Ara S, Ishaq MT, Sughra K. Green fabrication of copper oxide nanoparticles: a comparative antibacterial study against gram-positive and gram-negative bacteria. *Arab J Sci Eng*. 2022;47(1):523–33. <https://doi.org/10.1007/s13369-021-05767-5>.
- Gupta AK, Naregalkar RR, Vaidya VD, Gupta M. Recent advances on surface engineering of magnetic iron oxide nanoparticles and their biomedical applications. *Fut Med*. 2007;2:23–39. <https://doi.org/10.2217/17435889.2.1.23>.
- Han L, Zhan W, Liang X, Zhang W, Huang R, Chen R, et al. In-situ generation Cu₂O/CuO core-shell heterostructure based on copper oxide nanowires with enhanced visible-light photocatalytic antibacterial activity. *Ceram Int*. 2022;48(15):22018–30. <https://doi.org/10.1016/j.ceramint.2022.04.192>.
- Haque F, Rahman MS, Ahmed E, Bakshi PK, Shaikh AA. A cyclic voltammetric study of the redox reaction of Cu (II) in presence of ascorbic acid in different pH media. *Dhaka Univ J Sci*. 2013;61(2):161–6.
- Harish, Kumari S, Parihar J, Akash K, et al. Synthesis, characterization, and antibacterial activity of calcium hydroxide nanoparticles against gram-positive and gram-negative bacteria. *ChemistrySelect*. 2022;7(37):e202203094. <https://doi.org/10.1002/slct.202203094>.
- Hassan Afandy H, Sabir DK, Aziz SB. Antibacterial activity of the green synthesized plasmonic silver nanoparticles with crystalline structure against gram-positive and gram-negative bacteria. *Nanomaterials* [internet]. 2023;13(8):1327.
- Hofer UJNRM. The cost of antimicrobial resistance. *Nat Rev Microbiol*. 2019;17(1):3–3. <https://doi.org/10.1038/s41579-018-0125-x>.
- Huang C-W, Wu Y-T, Hu C-C, Li Y-Y. Textural and electrochemical characterization of porous carbon nanofibers as electrodes for supercapacitors. *J Power Sources*. 2007;172(1):460–7. <https://doi.org/10.1016/j.jpowsour.2007.07.009>.
- Jawad AS, Thewaini QN, Al-Musawi S. Cytotoxicity effect and antibacterial activity of Al₂O₃ nanoparticles activity against streptococcus pyogenes and proteus vulgaris. *J Appl Sci Nanotechnol*. 2021;1(3):42–50. <https://doi.org/10.5329/jasn.2021.3944.1061>.
- Jeevanandam J, Kiew SF, Boakye-Ansah S, Lau SY, Barhoum A, Danquah MK, et al. Green approaches for the synthesis of metal and metal oxide nanoparticles using microbial and plant extracts. *Nanoscale*. 2022;14(7):2534–71. <https://doi.org/10.1039/D1NR08144F>.
- Kamali F, Faghihi K, Mirhoseini F. High antibacterial activity of new eco-friendly and biocompatible polyurethane nanocomposites based on Fe₃O₄/Ag and starch moieties. *Polym Eng Sci*. 2022;62(5):1444–62. <https://doi.org/10.1002/pen.25934>.
- Kannan K, Radhika D, Nikolova MP, Sadasivuni KK, Mahdizadeh H, Verma U. Structural studies of bio-mediated NiO nanoparticles for photocatalytic and antibacterial activities. *Inorg Chem Commun*. 2020;113: 107755. <https://doi.org/10.1016/j.inoche.2019.107755>.
- Karimi M, Kashi MA, Montazer AH. Synthesis and characterization of ultrafine γ-Al₂O₃: Cr nanoparticles and their performance in antibacterial activity. *J Sol-Gel Sci Technol*. 2021;99(1):178–87. <https://doi.org/10.1007/s10971-021-05557-3>.
- Karuppannan SK, Ramalingam R, Mohamed Khalith SB, Dowlath MJH, Darul Raiyaan GI, Arunachalam KD. Characterization, antibacterial and photocatalytic evaluation of green synthesized copper oxide nanoparticles. *Biocatal Agric Biotechnol*. 2021;31: 101904. <https://doi.org/10.1016/j.bcab.2020.101904>.
- Khosravi MD, Ghahari M, Shafiee Afarani M, Arabi AM. Synthesis of CuO and CuO/ZnO composite powders for antibacterial, photocatalytic, and pigment-related applications. *Adv Ceram Prog*. 2022;8(1):1–8. <https://doi.org/10.3050/acp.2022.329820.1082>.
- Khusnuriyalova AF, Caporali M, Hey-Hawkins E, Sinyashin OG, Yakharov DG. Preparation of cobalt nanoparticles. *Eur J Inorg Chem*. 2021;2021(30):3023–47.
- Mahlambi PN, Moloto MJ. Starch-capped silver oxide (Ag₂O) nanoparticles: synthesis, characterization and antibacterial activity. *Dig J Nanomater Biostructures*. 2022;17:921–30.
- Monshi A, Foroughi MR, Monshi MR. Modified Scherrer equation to estimate more accurately nano-crystallite size using XRD. *World J Nano Sci Eng*. 2012;2(3):154–60.
- Moumen A, Fattouhi M, Abderrafi K, El Hafidi M, Ouaskit S. Nickel colloid nanoparticles: synthesis, characterization, and magnetic properties. *J Cluster Sci*. 2019;30(3):581–8. <https://doi.org/10.1007/s10876-019-01517-8>.
- Ogunyemi SO, Zhang M, Abdallah Y, Ahmed T, Qiu W, Ali MA, et al. The biosynthesis of three metal oxide nanoparticles (ZnO, MnO₂, and MgO) and their antibacterial activity against the bacterial leaf blight pathogen. *Front Microbiol*. 2020;11: 588326.
- Rashidi Ranjbar Z, Akbari Z, Khaleghi M. Synthesis, characterization, and antibacterial activities of Ag₂O nanoparticle and silver (I) nano-rod complex. *Nanochem Res*. 2020;5(2):233–40. <https://doi.org/10.22036/nrc.2020.02.013>.
- Saidin S, Jumat MA, Mohd Amin NAA, Saleh Al-Hammadi AS. Organic and inorganic antibacterial approaches in combating bacterial infection for biomedical application. *Mater Sci Eng, C*. 2021;118: 111382. <https://doi.org/10.1016/j.msec.2020.111382>.
- Saravanan A, Maruthapandi M, Das P, Luong JHT, Gedanken A. Green synthesis of multifunctional carbon dots with antibacterial activities. *Nanomaterials*. 2021;11(2):369. <https://doi.org/10.3390/nano11020369>.
- Sarian FD, Ando K, Tsurumi S, Miyashita R, Ute K, Ohama T. Evaluation of the growth-inhibitory spectrum of three types of cyanoacrylate nanoparticles on gram-positive and gram-negative bacteria. *Membranes* [internet]. 2022;12(8):782.
- Shaaban MT, Zayed M, Salama HS. Antibacterial potential of bacterial cellulose impregnated with green synthesized silver nanoparticle against *S aureus* and *P aeruginosa*. *Curr Microbiol*. 2023;80(2):75. <https://doi.org/10.1007/s00284-023-03182-7>.
- Shi X, Xu Z, Han C, Shi R, Wu X, Lu B, et al. Highly dispersed cobalt nanoparticles embedded in nitrogen-doped graphitized carbon for fast and durable potassium storage. *Nano-Micro Lett*. 2021;13:1–12.
- Sun B, Wu F, Zhang Q, Chu X, Wang Z, Huang X, et al. Insight into the effect of particle size distribution differences on the antibacterial activity of carbon dots. *J Colloid Interface Sci*. 2021;584:505–19. <https://doi.org/10.1016/j.jcis.2020.10.015>.
- Tian M, Dong C, Cui X, Dong Z. Nickel and cobalt nanoparticles modified hollow mesoporous carbon microspheres catalysts for efficient catalytic reduction of widely used dyes. *RSC Adv*. 2016;6(101):99114–9. <https://doi.org/10.1039/C6RA22498A>.

- Tran NT, Ha D, Pham LH, Vo TV, Nguyen NN, Tran CK, et al. Ag/SiO₂ nanoparticles stabilization with lignin derived from rice husk for antifungal and antibacterial activities. *Int J Biol Macromol*. 2023;230: 123124. <https://doi.org/10.1016/j.ijbiomac.2022.123124>.
- Wang L, Ali J, Zhang C, Mailhot G, Pan G. Simultaneously enhanced photocatalytic and antibacterial activities of TiO₂/Ag composite nanofibers for wastewater purification. *J Environ Chem Eng*. 2020;8(1): 102104. <https://doi.org/10.1016/j.jece.2017.12.057>.
- Wu ZG, Munoz M, Montero O. The synthesis of nickel nanoparticles by hydrazine reduction. *Adv Powder Technol*. 2010;21(2):165–8. <https://doi.org/10.1016/j.appt.2009.10.012>.
- Wu X, Xing W, Zhang L, Zhuo S, Zhou J, Wang G, et al. Nickel nanoparticles prepared by hydrazine hydrate reduction and their application in supercapacitor. *Powder Technol*. 2012;224:162–7. <https://doi.org/10.1016/j.powtec.2012.02.048>.
- Xiao X, He E-J, Lu X-R, Wu L-J, Fan Y-Y, Yu H-Q. Evaluation of antibacterial activities of silver nanoparticles on culturability and cell viability of *Escherichia coli*. *Sci Total Environ*. 2021;794: 148765. <https://doi.org/10.1016/j.scitotenv.2021.148765>.
- Yang S-Z, Liu Q-A, Liu Y-L, Weng G-J, Zhu J, Li J-J. Recent progress in the optical detection of pathogenic bacteria based on noble metal nanoparticles. *Microchim Acta*. 2021;188(8):258. <https://doi.org/10.1007/s00604-021-04885-z>.
- Zangeneh Kamali K, Alagarsamy P, Huang NM, Ong BH, Lim HN. Hematite nanoparticles-modified electrode based electrochemical sensing platform for dopamine. *Sci World J*. 2014;2014: 396135. <https://doi.org/10.1155/2014/396135>.
- Zhang X, Zhang G, Chai M, Yao X, Chen W, Chu PK. Synergistic antibacterial activity of physical-chemical multi-mechanism by TiO₂ nanorod arrays for safe biofilm eradication on implant. *Bioactive Mater*. 2021;6(1):12–25. <https://doi.org/10.1016/j.bioactmat.2020.07.017>.

Publisher's Note

Springer Nature remains neutral with regard to jurisdictional claims in published maps and institutional affiliations.